A Probabilistic Model-aided Failure Prediction Approach for Operating Mechanism of High Voltage Circuit Breakers

A. A. Razi-Kazemi, *Member, IEEE*, K. Niayesh, *Senior Member, IEEE*, R. Nilchi

***Abstract*— In order to avoid failures in circuit breakers (CBs) and to extend the lifetime of these critical components, condition-based-maintenance has been increasingly requested by utilities to enable them to efficiently manage their assets. The origin of the most failures in CBs is the operating mechanism. Travel curve (TC) could effectively reveal the condition of the operating mechanism. However, the measurement of a TC profile is not simple in all CBs. This paper presents the impacts of common failure modes of CBs on TC profiles, and proposes a new model-aided approach to simulate the behavior of the operating mechanism with coupling the model-based and rule-based approaches. The simulation results along with experiments conducted on 72.5 kV SF_6 CBs are organized into a fuzzy-probabilistic approach through maximum likelihood and interacting multiple models (IMM) to precisely predict the condition of CB and to detect intelligently the cause of the failure. For this purpose, the CB condition has been categorized into three modes based on its operating speed: normal (about 3 m/s), faulty #1 (less than normal range) and faulty #2 (more than normal rang). The mode variations of the CB have been estimated via IMM in each operation. The proposed approach in prediction of the failures and cause(s) prior to their occurrence has been verified against experiments.**

***Index Terms*— Circuit breaker (CB), condition-based maintenance, diagnostic, travel curve, probabilistic model.**

I. Introduction

Circuit breakers (CBs) are important and critical components to provide a safe and reliable network. Security, resiliency and stability of power systems are completely dependent on the reliable operation of CBs. Various maintenance strategies have been conducted by utilities for CBs to extend their lifetime and to avoid the failures [1]-[4]. As international surveys report, 50% to 52% of the major failures are of a mechanical origin [3]-[8], most researches have assessed the condition of CBs through operating mechanism based on various signals such as coil current, vibration and travel curve (TC). The formers are an indirect real-time method, while the TC is a direct method depending on the type of breakers could be applied online or offline. Literatures have tackled this subject from various perspectives such as failure identification, de-noising, modeling, etc. Reference [5] presents a mechanical status identification method based on covariance matrix that is used to get mechanical characteristic signals from the contact TC. In [6], radial basis function (RBF) neural network has been used as a recognition tool for fault diagnosis of CBs based on vibration signals. References [7] uses support vector machine to predict the TC and coil current. However, this paper could not provide a link between failures and signals. In [8]-[11], mechanical diagnosis is established based on the recorded vibration signals for SF_6 CBs using wavelet and vector-machine theory for diagnosing mechanical characteristic fault. Reference [12] addresses the correlation between TC and auxiliary contact to assess the condition of CBs. In [3], [13]-[15], coil current has been used to assess the control and mechanical section of CBs. Real-time assessment of operating mechanism through TC have been employed in some monitoring tools. Reference [16] presents two monitoring systems (CBWatch-1 and CBWatch-2) for CBs. The earlier assesses the gas density of CBs, while the latter can monitor mechanical and switching operation. It uses conventional auxiliary switches, static auxiliary switches or primary contact travel sensors. Reference [17] introduces another commercial condition monitoring units, where comb or optical travel sensors installed inside the mechanism (or close to the mechanism linkage) are employed to measure contact travel. The other online monitoring systems have been developed in [18], and [19] to monitor the mechanical characteristics of CBs. Noteworthy is that the measurement of TC requires transducer (linear/rotatory) attachment to CBs, which leads to some difficulties for online approach in some type of CBs. In [20], a real-time measurement for the moving displacement of a circuit breaker contact is presented to obtain contact stroke. In [21], a utility model including coil current and TC signal has been proposed to automatically monitor the condition of the CBs.

Most researches in this subject have been established based on vibration signals or coil current as an indirect method. However, they provide a weaker link to the operating mechanism in comparison with TC. In addition, the vibration signals could include noises and consequently a precise feature extraction method is required. Furthermore, many sensors need to be attached to the CBs to reach a reliable result; this leads to a cost increase. In addition, coil current could not assess some important parts such as damper or spring. For researches dealing with diagnostic methods based on TC, some shortcomings, and new challenges have been appeared. They need to be established based on experiments and be verified against intentional failures. In addition, the methods should employ diagnostic features that could cover common failure modes. Moreover, they should be compatible with smart grids

…..

and consequently they need to predict the condition of CBs and failure modes in addition to an intelligent assessment of the present condition. All of these have not been addressed within one framework yet. In response to these, the proposed method in this study is established based on the diagnostic features extracted from TC such as speed and over travel. It provides a strong link between mechanical operating mechanism of CBs and failures. A model-aided approach is taken in this paper to assess the condition of mechanism of CBs. Model aided diagnosis provides the best knowledge about the systems, which serves the aims of fault detection, localization, and the cause of faults and their assessment, and predictions [22], [23]. This paper couples the rule (expert)-based approach with the model-based approach to reach an intelligent methodology. For this purpose, impact of common failures on the characteristics of TCs in the spring drive mechanism is investigated through experiments and simulations. Regarding the simulation results and measurements, the effective diagnostic features have been developed based on the TCs profiles. Subsequently, the final database has been classified based on maximum likelihood into faulty and healthy cases, and a condition prediction approach has been established based on interacting multiple model (IMM) estimator. Furthermore, in the light of the model-aided and experimental results, the paper proposes a fuzzy-probabilistic approach to detect the failure modes and quantify intelligently the condition of CBs. The proposed framework has been established and verified based on the recorded signals from 72.5 kV, SF_6 CBs equipped with spring drive mechanism.

II. Model Description

The goal of this section is to clarify the developed dynamics model of operating mechanism through TCs to simulate the operation condition of the breaker under different fault. This information could provide great insight into the condition of various parts of drive mechanism such as closing and opening spring, damper, as well as motor used for charging and timing.

A. Linkage between Travel Curve and Operating Mechanism

Operating mechanism is comprised of a charging motor, a charging gear, an opening coil, a closing coil, an opening spring, a closing spring, a cam plate, and a coupling linkage. TC is a prominent signal, which could provide a strong linkage with mechanism. To give an illustration, a captured close/open TC profile is shown in Fig. 1. The resistive linear/rotatory displacement transducer is usually employed to record the TC. In the present study, as shown in Fig. 1, the rotary transducer has been employed to capture TCs.

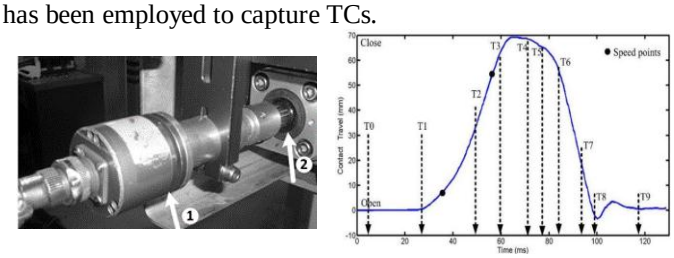

Fig. 1. Right: A recorded close-open T.C. profile, left: 1: rotatory transducer 2: main shaft.

Once a close command is sent by the protection relay/operator, the close coil is energized and converts the electrical command to the mechanical action at time, T0. The armature surrounded by the coil hits the latch; subsequently the stored energy in the closing spring is released and transferred to the contacts through the coupling linkage. The required time for all these actions is indicated by T1. At time T2, the moving contact reaches the fixed contact. The CB reaches its closed position at time T3. There are some oscillations to settle the fixed position at time T4. Similar procedure is observed during trip operation. Trip coil is energized at T5. Subsequently, moving contacts start to move from closed position to open position at time T6. The opening action is completed following the time T7. At time T8, the moving contact goes back to the final open position. However, the final position has been reached at time T9 after some mechanical oscillation of moving contacts resulting from contact bouncing. The recorded TC profile provide valuable information regarding the timing of CBs as well as the condition of springs and damper. The operating speed of the CB is determined using time/displacement at two points on the TC. While one point can lie at a certain distance from the closed-position of CBs or the contact-closure/separation, the other is specified by a time interval from 10 to 20 ms (see Fig. 1) [12].

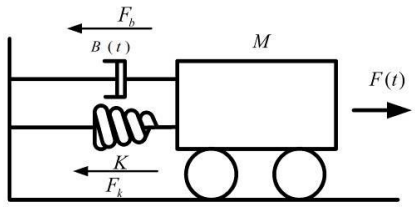

Fig. 2. Schematic of second-order system (mass, spring and damper) [24].

B. Travel Curve and Mechanical Second-order System

The operating mechanism explained in the previous section is modeled through a second-order free body system, comprising a spring and a damper attached to a mass, as shown in Fig. 2. The spring force is proportional to its displacement in *x*-direction, $F_k=kx$. Damping force provided by damper is proportional to velocity in *x*-direction, $F_b=bdx/dt$. In these equations, *k* and *b* are spring constant (in N/m) and damping coefficient (in N-s/m), respectively. The dynamic state of the present system is characterized by following governing equation based on the Newton's second law [24].

$$-F_b - F_k + F(t) = -b\frac{dx}{dt} - kx + F(t) = m\frac{d^2x}{dt^2} \quad (1)$$

Using Laplace transform, the transfer function of the output signal *X(s)* to input signal *F(s)* is obtained as:

$$T(s) = \frac{X(s)}{F(s)} = \frac{1}{ms^2 + bs + k} \quad (2)$$

The input signal is applied force and the output signal is the displacement. The standard format of (2) is calculated as follows:

$$T(s) = K' \frac{\omega_n^2}{S^2 + 2\zeta\omega_n S + \omega_n^2} \quad (3)$$

As the system under study is generally under-damped [10], [24], its step response is as follows:

$$x(t) = 1 - e^{-\zeta\omega_n . t}\left(cos(\omega_d . t) + \frac{\zeta}{\sqrt{1-\zeta^2}} sin(\omega_d . t) \right) \quad (4)$$

The standard parameters are ζ, damping ratio; ω_d, the damped frequency; and ω_n, the natural frequency as presented in (5).

$$\zeta = \frac{b}{2\sqrt{m.k}} \tag{5-1}$$

$$\omega_n = \sqrt{\frac{k}{m}} \tag{5-2}$$

$$\omega_d = \omega_n\sqrt{1-\zeta^2} \Rightarrow \omega_d = \omega_n\sqrt{1-\frac{b^2}{4m.k}} \tag{5-3}$$

In order to estimate the standard parameters through the captured TCs, the time to overshoot (T_p) and the overshoot amplitude (P_o) have been employed as follows:

$$P_o = 100 \times e^{-\Pi\frac{\zeta}{\sqrt{1-\zeta^2}}} \tag{6-1}$$

$$T_p = \frac{\pi}{\omega_d} \tag{6-2}$$

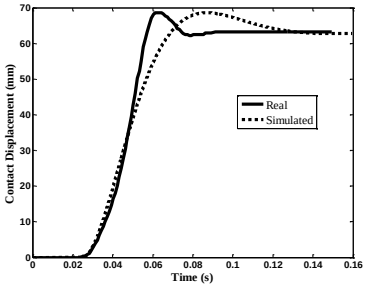

Fig. 3. Simulated T.C regarding the second order system and measured profile

C. Verification and Re-simulation

The mechanical behavior of a CBs has been simulated though the eqs (1)-(6). The simulation results and a recorded TC profile have been demonstrated in Fig. 3. As it can be seen, the simulation could not follow the real signal. The reason lies in the dynamic behavior of the damper used in CBs as shown in Fig. 4(a). It includes a cylindrical body filled by silicon oil. The damper parameter has been supposed to be constant. However, linear fluid viscous damper has been employed for suppression of high velocity shocks during opening operation of the CBs. This structure follows a behavior as shown in Fig. 4(b). Consequently, in order to address this fact, the dependency of the damper-profile to the displacement has been involved in the model using a time-varying damping ratio as shown in Fig. 4(b) through considering a linear function for damping ratio. In order to investigate this non-linear dynamic model within acceptable error, the linearization has been conducted per 100μs. As shown in Fig. 5, the simulated TC using the modified model follows the recorded travel curve.

D. Correlation between Damped Natural Frequency (ω_d) and Damping Ratio (ζ)

During the operation of CBs, the damper parameter has obtained small values and it increases with time. In addition, the damping ratio is proportional to the damper parameter. The following equation is calculated based on eq. 5-3:

$$\omega_d(t) = \omega_n\sqrt{1-\xi^2} = \sqrt{\frac{k}{m}(1-\frac{b(t)^2}{4\cdot m\cdot k})} \tag{7}$$

The derived equation indicates that the ω_d is inversely related to the damping ratio. Fig. 6(a) presents the time variations of damper ratio and the damped natural frequency during simulation. This is in agreement with the excepted reversal behavior in the reality.

E. Other Verification: Natural Frequency of the System

The fact that the natural frequency needs to be constant can be used to verify the dynamic model. For this purpose, the natural frequency of the proposed model has been recorded during the simulations (see Fig. 6(b)). As it can be seen, the natural frequency in the proposed model is constant during simulations.

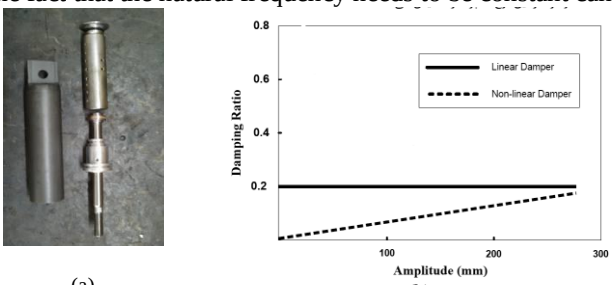

(a) (b)

Fig. 4. (a): Cylindrical damper with radial holes used in CBs (b): Damping ratio of in damper-spring system with non-linear damper.

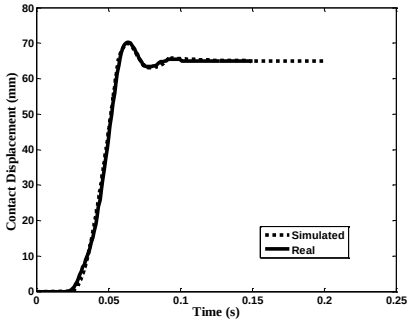

Fig. 5. Simulated T.C regarding the second order system considering non-linear behavior of the damper.

III. Failures and TC Characteristics

In order to obtain important features of TC for diagnosis of CBs, this section is devoted to clarify the impacts of failures on the characteristics of TC profile (signal and knowledge identification). Data is gathered from 300 tests conducted on 12 puffer type 72.5 kV SF_6 CBs, equipped with spring drive mechanism in Pars Switch Co. The recorded profiles include healthy and non-healthy TCs obtained from CBs with intentional failures dealing with four type common failures. As the implantation of intentional failures are a difficult task, the information presented here is helpful for establishment of a

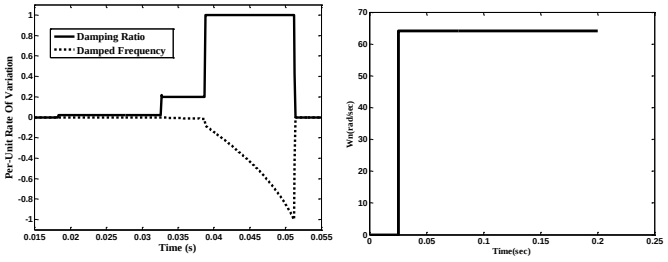

(a) (b)

Fig. 6. a) Damping ratio and frequency versus time b) variations of natural frequency during simulation.

diagnosis approach as well as from general viewpoint of diagnosis of the CBs.

A. on/off Switch of Motor Used for Spring Charging

Subsequent to the trip command, the closing spring would be fully charged by the motor. As shown in Fig. 7(a), a mechanical switch is employed to detect the full level charge and subsequently to disconnect the voltage source from the motor. The common failures in this switch include dislocation and short-circuit of switch resulting from vibration during operation, aging, etc.

The common failure modes resulted from the malfunction in this part are as follows:

I) while the CB receives the closing command, it does not operate (See Fig. 7(b))

II) CB could not complete the close operation (See Fig. 7(c))

B. Trip/Close Coil

As mentioned earlier, the CBs are equipped with two coils for trip and close operation. The main objective of this part is to convert electrical signals to the mechanical actions. Fig. 8(a) shows the close coil (A) and trip coil (B). Various failures may happen in coils such as latch malfunction, short-circuit in coils, low/high DC input voltage and stiffness of the latch. These failures could affect the timing parameters of CBs and result in lengthier trip/close time, no-operation in spite of receiving trip/close command, operation in spite of receiving no command of trip/close. Fig. 8(b) presented the delay time in opening operation resulting from trip coil failure. More information regarding the failures of this component is available in [14].

C. Closing and Opening Spring

Various drive mechanism such as spring, hydraulic and pneumatic drives are employed in CBs, amongst them, spring drive mechanism is increasingly used in CBs giving rise to its high reliability, and simplicity. Failures in this part are as follows: non-complete charge of spring resulting from the

(a)

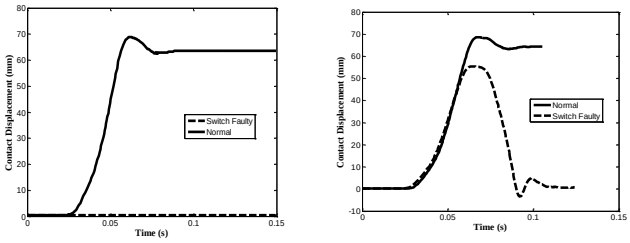

(b) (c)

Fig. 7. a) Spring Charging Switch (auxiliary contact S_3); b) and c) The T.C. profile of the common failures in spring charging switch.

(a)

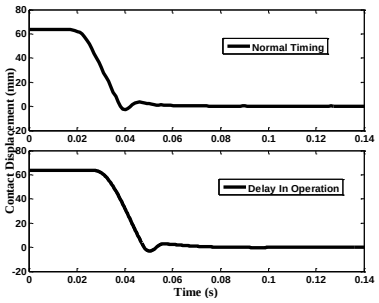

(b)

Fig. 8. a) A: closing coil B: opening coil; b) Normal and faulty T.C. profile regarding the failure in opening coil.

malfunction in charging motor, environmental impacts, as well as the increase of initial length of spring resulted from longtime inactivity of CBs. Fig. 9(a) illustrates the closing spring (A) and opening spring (B) in a 72.5 kV CB.

Any failures on the charging of spring could lead to a direct impact on the operation speed and timing of CB. Standards define that the closing and opening time need to lie within 45-57 ms, and 23-32 ms, respectively [3]. The changes in the initial length of spring could change the total stroke of CBs, which should be within 63-67 mm. Fig 9 (b) and (c) present the healthy and faulty TC profile resulting from a low-charged spring.

D. Damper

In order to absorb extra energy released by the spring and to damp overshoot and undershoot of the contact traveling, a damper is used in the operating mechanism of CBs as shown in Fig. 10(a). The common failures in this part are comprised of oil leakage, deterioration of piston due to friction and the decrease of oil viscosity. The heat resulting from high operation frequency decreases the oil viscosity and consequently the decrease of damping factor. The condition of damper could

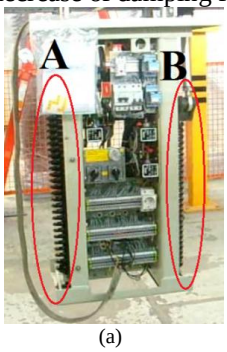

(a)

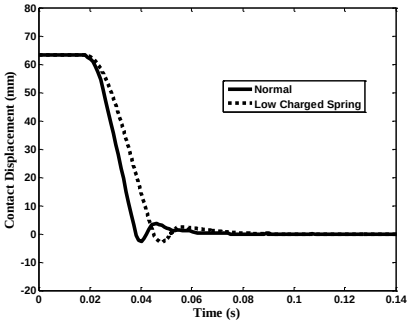

(b)

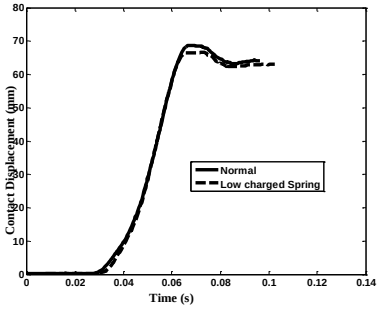

(c)

Fig. 9. a) A: Closing Spring B:Opening Spring; b) Impact of opening spring failure on T.C. profile-simulation result; c) closing spring falure on T.C. profile-experiment.

TABLE I. DIAGNOSIS FEATURES AND FAILURE CAUSES

Faulty Parameter	Reason			
Timing	Spring	Latch	Coil	Friction
Speed	Spring	Friction	Damper	
Stroke	Filler		Spring length	
Over Travel	Damper	Spring	Contact Not adjust	

effectively be attributed through the operation speed and the maximum overshoot of T.C. profile. Standards define that the maximum overshoot should be 2-6 mm and 5 mm for closing and opening operation, respectively [12]. The impact of damper malfunction on oscillations of T.C. profile has been illustrated in Fig. 10(b). Table I presents the common failures and their causes in CBs within one framework.

IV. Condition Prediction based on Probabilistic-Approach

The chart shown in Fig. 11 presents how a complete database has been provided both through experiments and by application of the developed model, and all steps to reach the final probabilistic model-aided diagnostic approach. Noteworthy is that the presented approach is independent of the CB type, however the target CB here is SF_6, 72.5 kV. The initial database, a set of 300 TC profiles, is provided based on experiments conducted on 12 CBs. Subsequently, the behavior of operating mechanism has been modeled by a second order model with respect to time-varying damping ratio as explained in section II. The main diagnostic parameters have been discussed in section III based on the recorded and simulated profiles resulting from the developed model. The secondary database has been constructed regarding the four diagnostic parameters, i.e. timing, speed, stroke, and over travel as presented in Table I. The diagnostic features in the secondary database are classified into three modes, i.e. normal, faulty#1 and faulty#2 based on maximum likelihood (ML) method as explained in this section. The classified data and subsequently the fitted probability distribution functions construct the final database as the prior knowledge of IMM estimator and fuzzy approach for the condition prediction and failure(s) cause detection, respectively. In order to predict the condition of the CBs, IMM estimator has been used to involve both rule-based and model-based approach. The IMM estimator has been recognized as the most cost-effective and simple approach for the state estimation in hybrid systems. It enables one to precisely estimate the state of dynamic-systems with several behavior modes [25], [26]. The methodology is comprised of three main sections: assessment of present condition of the CB (IV-A), condition estimation of CB for next operation (IV-B) and the failure cause identification (V).

A. Classification based on Maximum Likelihood (ML)-Condition assessment

ML as a most popular method of the classification is employed to organize the database obtained through

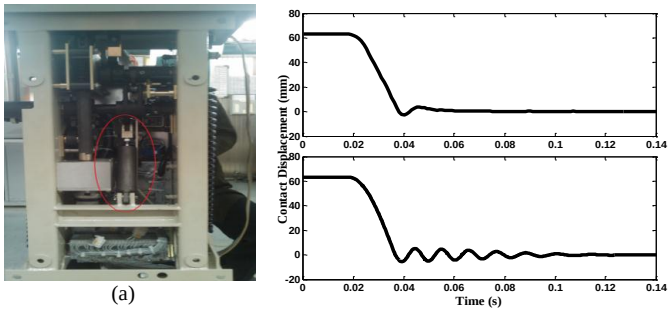

(a) (b)

Fig. 10. a) Damper of 72.5 kV CB; b) Impact of the decrease of damping ratio on TC profile.

experiments and the developed model into meaningful classes, i.e. normal and faulty. In order to define those, the classes have been generally defined through (8):

$$C=\{C_1,C_2,...,C_{nc}\} \tag{8}$$

where, *nc* is number of classes. The likelihood of class C_i is defined as follows:

$$P(C_i|x)=P(x|C_i)\times P(C_i)/P(x) \tag{9}$$

where

$P(C_i|x)$: The posterior probability of a data *x* belonging to the class C_i, $P(x|C_i)$: Conditional probability to observe *x* from the class C_i, or probability density function, $P(C_i)$: is the priori information, i.e., the probability that class C_i occurs in the study area

$P(x)$: is the probability that *x* is observed, which can be written as:

$$P(x)=\sum_{i=1}^{n_c}P(x|C_i)\times P(C_i) \tag{10}$$

As the diagnostic features under healthy and faulty conditions in high voltage CBs follow normal distributions [12], in the light of normal probability density function, $P(x|C_i)$ can be expressed as follows:

$$P(x|C_i)=\frac{1}{\sqrt{2\pi}\times\delta_i}\times\exp\left\{-\frac{(x-\mu_i)^2}{2\delta_i^2}\right\} \tag{11}$$

where δ_i and μ_i are standard deviation and mean value of the data in i^{th} class, C_i [25]. A feature could lie within normal or faulty range. In addition, a feature, in a fault case, could be larger or smaller than its normal range. Consequently, three classes have been considered in this paper. To give an illustration, the ML-based classifier is implemented for dataset corresponding to the diagnostic feature "over travel" via (9). Figs. 12(a), (b) and (c) show the training dataset obtained from the secondary database and normal probability distributions, respectively. The obtained classifier via ML method for dataset corresponding to this feature is shown Fig. 12(d). The similar procedure has been conducted for other features to identify the classifiers. The final database including these classified data set is served as the prior knowledge of IMM to estimate the condition of CB and as the useful knowledge to propose proper membership functions for the failure cause detection via fuzzy approach. In addition, it helps us to assess the present condition of the CBs via (15) as explained in section IV.C.

B. Condition Assessment of CB: Mode (Condition) Prediction

Three modes have been defined for the condition of CBs as follows: normal, failure #1 (more than normal range), and

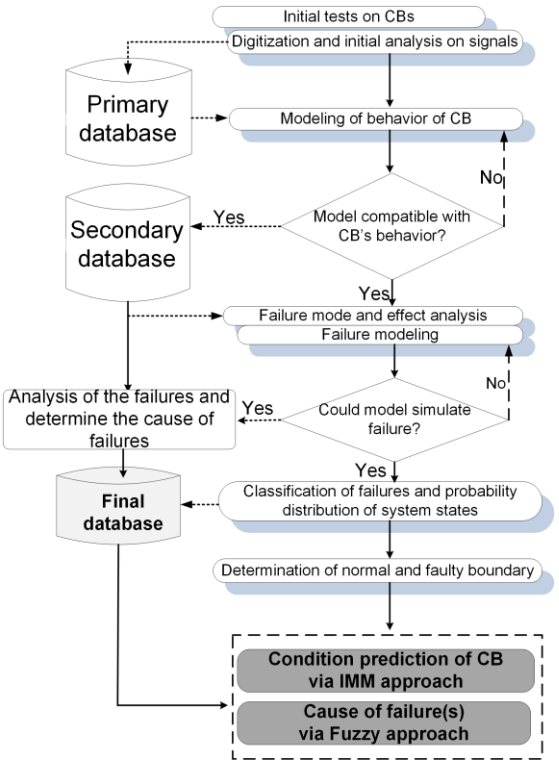

Fig. 11: Outline of the proposed approch.

failure #2 (less than normal range). The IMM estimator as the state-of-the-art technique for tracking maneuvering targets has employed to predict the condition of CB regarding the defined modes as explained as follows [25], [26]:

The system could follow one of *r* modes (or conditions) as expressed generally as follows:

$$M=\{M_j\}_{j=1}^{r} \tag{12}$$

In the present work, *r* is three, i.e. normal (M_1), faulty #1 (M_2) and faulty #2 (M_3). The prior probability that the CB is in mode *j* is:

$$P\{M_j \mid Z^0\}=\mu_j(0) \quad j=1,2,3 \tag{13}$$

where Z^0 is the prior information and

$$\sum_{j=1}^{3}\mu_j(0)=1 \tag{14}$$

The posterior probability of the condition (mode) *j* being correct ($\mu_j(k)$), given the measurement data up to *k* (Z^k), is given by the recursion using Bayes formula:

$$\begin{aligned}\mu_j(k)&\overset{\Delta}{=}P\{M_j \mid Z^k\}=P\{M_j \mid z(k),Z^{k-1}\}\\&=\frac{p[z(k)\mid Z^{k-1},M_j]P\{M_j \mid Z^{k-1}\}}{p[z(k)\mid Z^{k-1}]}\\&=\frac{p[z(k)\mid Z^{k-1},M_j]P\{M_j \mid Z^{k-1}\}}{\sum_{i=1}^{3}p[z(k)\mid Z^{k-1},M_i]P\{M_i \mid Z^{k-1}\}}\end{aligned} \tag{15-1}$$

or

$$\mu_j(k)=\frac{p[z(k)\mid Z^{k-1},M_j]\mu_j(k-1)}{\sum_{i=1}^{3}p[z(k)\mid Z^{k-1},M_i]\mu_i(k-1)},\quad j=1,2,3 \tag{15-2}$$

Starting with the given prior probabilities (13).

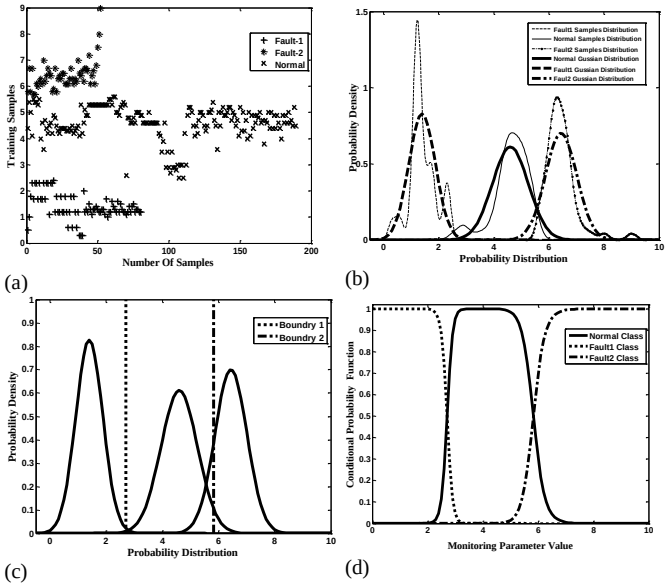

Fig. 12. (a) training samples for classification (b) density distribution and the fitted normal probability distribution function, (c) classified of the dataset and determination via ML and (d) $P(C_1|x)$, $P(C_2|x)$ and $P(C_3|x)$.

One cycle of the IMM consists of the following steps:

I) Calculation of the mixing probabilities (i, j=1, 2, 3):

The probability that mode M_i was in effect at *k*-1 given that M_j is in effect at *k* conditioned on Z^{k-1} is

$$\begin{aligned}\mu_{i|j}(k-1\mid k-1)&\overset{\Delta}{=}P\{M_i(k-1)\mid M_j(k),Z^{k-1}\}\\&=\frac{1}{\bar{c}_j}P\{M_j(k)\mid M_i(k-1),Z^{k-1}\}P\{M_i(k-1)\mid Z^{k-1}\}\end{aligned} \tag{16}$$

The above are the mixing probabilities, which can be written as:

$$\mu_{i|j}(k-1\mid k-1)=\frac{1}{\bar{c}_j}p_{ij}\mu_i(k-1),\ i,j=1,2,3 \tag{17}$$

Where p_{ij} and $\bar{c}_j$ are the mode transition probability and normalizing constant, respectively. Normalizing constants are given as:

$$\bar{c}_j=\sum_{i=1}^{3}p_{ij}\mu_i(k-1),\ j=1,2,3 \tag{18}$$

As it can be deduced, the change condition ($\mu_{i|j}$) is dependent on the history of CBs, which is compatible with reality. $\mu_{i|j}$ indicates the change of CB mode from *i* (in present operation) to *j* (in next operation).

II) Mode-matched filtering

In this step, the likelihood of modes in k^{th} observation has been calculated based on normal distributions and conditional probabilities using eqs. (8) to (11).

III) Mode probability update

The posterior probability of the condition (mode) *j* ($\mu_j(k)$) is updated as follows:

$$\begin{aligned}\mu_j(k)&=\frac{1}{c}L_j(k)\sum_{i=1}^{3}p_{ij}\mu_i(k-1),\ j=1,2,3\\c&=\sum_{j=1}^{3}L_j(k)\bar{c}_j\end{aligned} \tag{19}$$

The interested reader is referred to [25], [26] for a more comprehensive review of IMM and other probabilistic approaches.

C. Verifications through Experiments: Case Studies

In this part, using two case studies it is demonstrated how the IMM approach could assess the present condition of CB and how it could predict the condition of the CB in the next operation. The boundaries have been identified based on the classification approach explained in section IV.A. Fig. 13(a) presents the conditional probability calculated via (11). As it can be seen, speeds within [2.8-3.28] m/s are normal, which is in agreement with practice. Ten recorded-speeds of a SF_6 CB for its ten subsequent operations have been employed to check the feasibility and applicability of the model as presented in Table II. The likelihood of conditions (modes) for each operation is shown in Fig. 13(b). The values related to each operation has been obtained based on the conditional probability shown in Fig. 13(a). Table II presents quantitatively the likelihood of operation modes shown in Fig. 13(b). To give an illustration, for operation #1, the probability of modes 1 (normal), 2 (faulty #1) and 3 (faulty #2) are 0.94, 0.021, and 0.033, respectively. It indicates that the CB is most probably in healthy (state) condition in the operation #1. This condition assessment corresponds to the CB's real condition as a speed of 3.1 m/s lies within the normal range. Fig. 13(b) and Table II indicate that the CB condition is transiting from the normal mode to the faulty #1 mode. The mode of the CB is #1 (normal) up to the 5th operation. In the next operations, the CB is transiting to mode #1 (faulty #1) such that it clearly changes in 7th operation from the normal to the faulty#1 mode.

Following explanations clarify how the IMM approach could estimate the next condition of the CB in each operation based on previous data. Mixing probabilities given in (16) to (18) enable us to predict the next operation condition. In the present case, $\mu_{5|6}$ and $\mu_{6|7}$ have been calculated as follows:

$$\mu_{5|6} = \begin{bmatrix} 0.076 \rightarrow M_1 : normal \\ 0.67 \rightarrow M_2 : faulty\#1 \\ 0.25 \rightarrow M_3 : faulty\#2 \end{bmatrix}; \mu_{6|7} = \begin{bmatrix} 0.001 \\ 0.81 \\ 0.20 \end{bmatrix}$$

The mixing probability $\mu_{5|6}$ indicates that the probability of transiting to mode #2 (faulty #1) is 0.67 for 6th operation based on the available information up to 5th operation. Similarly, $\mu_{6|7}$ refers to the fact that the probability of entrance to mode #2 for 7th operation is about 0.81. Consequently, prediction of estimator from the condition of CB in 5th and 6th operation for next operation is "the entrance of CB mode to faulty#1". This shows how the implementation of IMM approach could effectively and precisely predict the condition of CBs prior to a failure (prediction of failure in 5th operation). Using an intelligent approach like this, the costs related to failures and maintenance of CBs may be drastically reduced. In addition, the results reveal the accuracy of the predictor in condition assessment of the CB. The likelihoods dealing with the 6th and 7th operation in Table II verifies the results of estimator, as well. Practically approach, the speeds within 2.9 m/s to 2.4 m/s for the 5th to 10th operations reveal a malfunction in the drive mechanism of the CBs.

TABLE II. SAMPLE RECORDED DATA FOR VERIFICATION AND MEMBERSHIP PROBABILITY

Membership probability for classes	Speed(m/s)	#	Membership probability for classes	Speed(m/s)	#
0.5267			0.9495		
0.3514	**2.8**	**6**	0.0215	3.1	1
0.1219			0.0331		
0.0017			0.9920		
0.9038	**2.7**	**7**	0.0038	3	2
0.0945			0.0042		
0.0000			0.9924		
0.9774	2.6	8	0.0022	3.2	3
0.0226			0.0054		
0.0000			0.9944		
0.9931	2.5	9	0.0028	4	4
0.0069			0.0028		
0.0000			0.9683		
0.9967	2.4	10	0.0196	2.9	5
0.0033			0.0121		

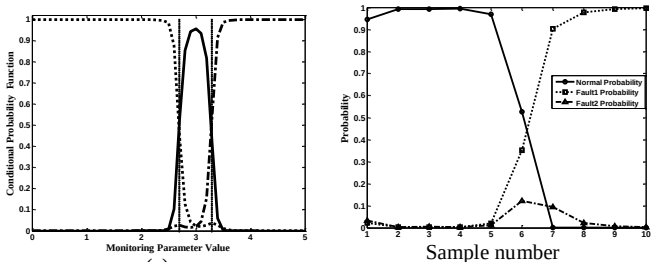

(a) (b)

Fig. 13. a) The conditional probability of membership for speed; b) The prediction of CB condition based on sample data.

The second case study is demonstrated in Fig. 14. Speeds listed for operations 1 to 3 and 7 to 10 are lower and upper than the normal range, respectively. The calculated conditional probabilities verify this observation. In addition, the calculated mixing probability, i.e. $\mu_{2|3} = [0.07 \;\; 0.66 \;\; 0.255]'$, indicates that in the second operation of the CB, the expected condition for next operation is faulty #1. As it can be seen in Fig. 14 for 3rd operation, this estimation is true and the CB is in mode #2 (faulty #1).

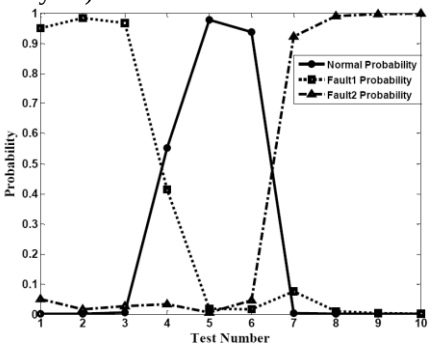

Speed (m/s)	#
2.4	1
2.6	2
2.8	3
3	4
3.1	5
3.3	6
3.5	7
3.6	8
3.7	9
3.8	10

Fig. 14: right: second cases study, left: conditional probability.

V. FAILURE CAUSE DETECTION BASED ON FUZZY-APPROACH

Once the condition of the CB is identified based on probabilistic approach, the other significant step in diagnosing

of CBs is detection of the cause(s) of failures. This section is devoted to build a failure cause detection model based on the expert's knowledge and results presented in previous sections through fuzzy approach.

The fuzzy system is established based on if/then rule between fuzzified inputs and outputs. Finally, the fuzzy outputs are deffuzified to be a crisp value. Table III presents the parameters of diagnosis and the possible contribution of various parts in faulty cases based on the expert knowledge. The fuzzification has been rectified based on the Gaussian curves resulted from IV-B. In order to cover all feasible failure modes, different major or minor failures during adjustment of the CBs have intentionally applied to the CBs such as trip/close coil failure, damper malfunction: oil leakage, malfunction in opening/closing spring. To give an illustration, the Fig. 12(d) or 13(a) could be applied as the membership functions related to the 'over travel' or 'speed' in fuzzification process. In addition, the Zadeh-inference engine has been applied in this work via (16) [27].

$$\mu_{B'}(y)=\max_{i=1}^{M}\left[\sup_{x\in U}(\mu_{A'}(x)\prod_{i=1}^{n}\mu_{A_i}(x_i)\mu_{B'}(y))\right] \quad (16)$$

The maximum probability of failure modes have been involved as the inputs of fuzzy system via (17):

$$P_{ERROR}=[Time_{Error},Speed_{Error},Stroke_{Error},Ov.Travel_{Error}] \quad (17)$$

To give an illustration, an error probability matrix is set as the input of fuzzy system as follows:

$$P_{ERROR}=\begin{bmatrix}0.3417 & 0.9442 & 0.0015 & 0.8609\end{bmatrix} \quad (18)$$

Table IV presents the output of fuzzy system regarding (18). The fuzzy system has realized that the failure is resulted from malfunction in spring and the second cause may be the damper operation. It is compatible with the real world due to this fact that the failure in the damper and spring could provide such profile as explained in III-C and III-D. As stated in Table I, malfunction in spring and dampers are the main origin of this type of failure. Modern smart power grids need intelligent algorithms to assess and predict the condition of CBs. Although conventional approaches could report and set a condition to CBs without any prediction or interpretation of the causes of the failures, they need a comprehensive database, which is usually rarely available in the utilities. Moreover, recorded signals under various faulty cases, which are the main requirement for a precise diagnosis, are difficult to apply in practice. With respect to the presented results, the proposed approach could effectively identify the condition of the CB and estimate the next operation mode through IMM. In addition, the results indicate that using fuzzy approach enables one to identify effectively the origin of failure(s). Noteworthy is that main disadvantages of such models is its dependency on the type of CBs. The new breakers from voltage level or design point view need a new model.

VI. Conclusion

In this paper, an extensive investigation on common failures in drive mechanism and TC profile of gas circuit breakers has been presented. Drive mechanism has been modeled by a second-order system with a time-varying damping ratio. The proposed modeling method enables to predict the condition of the operating mechanism of the circuit breaker based on the measured travel curve using a fuzzy-probabilistic approach. Moreover, it is possible to classify the condition of CB based on ML approach into three clusters: normal, faulty #1 and faulty #2. Implementation of the proposed approaches enables an efficient and precise prediction of the CB failures. The most probable fault causes of operating mechanisms are malfunction of spring, latch, coils and dampers. The results of the investigations in this paper show that the above-mentioned malfunctions can be revealed through features of the CB travel curve. Any changes in timing or speed is most likely an indication of a damaged spring, over travel of the CB travel curve is, in turn, most probably an indication of a failure in damper, and any change in rising time of the CB travel curve is most likely caused by a failure in coils of the operating mechanism.

Table III. The Role of values Parts of CBs on Faulty Parameter

Faulty Parameter	Reason			
Timing	Spring	Latch	Coil	Friction
	40%	20%	10%	10%
Speed	Spring	Friction	Damper	
	80%	15%	5%	
Stroke	Filler		Spring length	
	50%		50%	
Over Travel	Damper	Spring	Contact Not adjust	
	50%	40%	10%	
Rising Time	Coil	Friction	Auxiliary Contacts	
	50%	30%	20%	

Table IV. The Cause of Failure: Fuzzy System Output

Faulty Parameter	Spring	Latch	Contact Not adjusted	
Probability	**0.5948**	0.0329	0.0414	
Faulty Parameter	Friction	Filler	Damper	Coil
Probability	0.0845	0.0004	**0.2296**	0.0164

References

[1] E. A. Vianna, A. R. Abaide, L. N. Canha and V. Miranda, "Substations SF_6 circuit breakers: Reliability evaluation based on equipment condition," Electric Power Systems Research. 2017 Jan 31; 142: 36-46.

[2] X. Zhang, E. Gockenbach, Z. Liu, H. Chen and L. Yang, "Reliability estimation of high voltage SF_6 circuit breakers by statistical analysis on the basis of the field data," Electric Power Systems Research. 2013 Oct 31; 103: 105-13.

[3] A. A. Razi-Kazemi, M. Vakilian, K. Niayesh, and M. Lehtonen, "Data Mining of Online Diagnosed Waveforms for Probabilistic Condition Assessment of SF6 Circuit Breakers," IEEE Trans. Power Del., vol. 30, no. 3, pp. 1354 - 1362, 2015.

[4] K. Niayesh and M. Runde, *Power Switching Components: Theory, applications and future trends*, Berlin: Springer, 2017.
[5] J. Yang, B. Wu, Y. Wu, K. Zhao, H. Li, and G. Zhang, "High voltage circuit breaker dynamics simulation and mechanical state recognition," Proc. of IEEE Int. Conf. Elec. Materials and Power Equipment, pp. 406-409, May, 2017.
[6] L. Bing, L. Mingliang, Y. Ping, X. Yaowen, and P. Quanwei, "Machinery fault diagnosis method of HV circuit breaker based on EEMD and RBF neural network," Proc. of 29th IEEE Chinese Conf. Control and Decision Conference (CCDC), pp. 2115-2120, May, 2017.
[7] X. Zhang, R. Huang, S. Yao, G. Li, G., Zhong, L. and Wang, X., "Mechanical life prognosis of high voltage circuit breakers based on support vector machine," Proc. of 11th IEEE Chinese Conf. Natural Computation (ICNC), pp. 749-753, Aug. 2015.
[8] N. Charbkeaw, T. Suwanasri, and T. Bunyagul. "Mechanical defect detection of SF_6 high voltage circuit breaker using wavelet based vibration signal analysis," *in Proc*: Int. Conf. Electrical Engineering/Electronics, Computer, Telecommunications and Information Technology, vol. 2, IEEE, 2008.
[9] X. Zhang, "Mechanical life prognosis of high voltage circuit breakers based on support vector machine," Proc. of Int. Conf. Natural Computation, pp. 749 - 753, 2015.
[10] D. P. Hess,, S. Y. Park, M. K. Tangri, S. G. Vougioukas, A. Soom, V. Demjanenko, R. S. Acharya, D. M. Benenson, and S. E. Wright. "Noninvasive condition assessment and event timing for power circuit breakers," *IEEE Trans. Power Del.*, vol. 7, pp. 353-360, Jul. 1992.
[11] L. Xin, C. Chen, C., and X. Jian-yuan, "Research on fault diagnosis method of circuit breaker mechanical characteristics based on relevance vector machine," in Proc: Int. IEEE Conf. In Electric Power Equipment, Switching Technology (ICEPE-ST), 2015, pp. 606-610.
[12] A. A. Razi-Kazemi, "Applicability of Auxiliary Contacts in Circuit Breaker Online Condition Assessment," Electric Power Systems Research, vol. 128, pp. 53 – 59, Jun. 2015.
[13] S. M. Strachan, S. D. McArthur, B. Stephen, J. R. McDonald, and A. Campbell, "Providing decision support for the condition-based maintenance of circuit breakers through data mining of trip coil current signatures". *IEEE Trans. on Power Del.*, vol. 22, no. 1, pp.178-186, 2007.
[14] A. A. Razi-Kazemi, M. Vakilian, K. Niayesh, and M. Lehtonen, "Circuit-Breaker automated failure tracking based on coil current signature," IEEE Trans. Power Del., vol. 29, pp. 283-290, Feb. 2014.
[15] R. Peilei, J. Huang, X. Hu and J. Xiao, "Testing of circuit breakers using coil current characteristics analysis," Proc. of Int. Conf. Control and Automation, 2009, pp. 185-189.
[16] J. P. Dupraz, A. Schiemann, GF. Montillet, "Design objectives of new digital control and monitoring of high voltage circuit breakers" in Proc: IEEE Transmission and Distribution Conference and Exposition, PES, vol. 2, pp. 1088-1093, 2001.
[17] A. Poeltl, M. Haines, "Experiences with condition monitoring of HV circuit breakers" in Proc: IEEE Transmission and Distribution Conference and Exposition, PES, vol. 2, pp. 1077-1082, 2001.
[18] H. Xinbo, H. Xia, "Design of an on-line monitoring system of mechanical characteristics of high voltage circuit breakers" in Proc: IEEE International Conference Electronics, Communications and Control (ICECC), Sep. 9, pp. 3646-3649, 2011.
[19] H. Chunguang, C. Yundong, "Research on a novel on-line monitoring system for Mechanical Characteristic of Circuit Breaker" in Proc: IEEE Industrial Electronics and Applications, (ICIEA), May 25, pp. 3073-3076, 2009.
[20] C. Jiajia; C. Yaomin; C. Moyang; W. Yanlin, Circuit breaker contact stroke measuring method, CN107860291(A), 2018-03-30
[21] W. Wei; P. Qiang; Z. Dengfeng, Online monitoring device of high - voltage breaker, CN207114721(U), 2018-03-16
[22] M. S. Silva, J. A. Jardini, L. C. Magrini, A. Corvo, L. A. Solis, and F. Veiga. "Determination of the circuit breaker operation times using the wavelet transform," *in Proc:* IEEE Power Engineering Society General Meeting, pp. 1214-1219, 2004.
[23] M. Stanek, K. Fröhlich, "Model-aided diagnosis-a new method for online condition assessment of high voltage circuit breakers," *IEEE Trans. Power Del.*, vol. 15, pp. 585-591, 2000.
[24] E. Corona, "Dynamic Response of Measurement Systems", Measurements Laboratory, spring, 1999.
[25] J. Gomes, An overview on target tracking using multiple model methods. Master thesis, 2008, Institute Superior T´ecnico *Citeseer*.
[26] Y. Bar-Shalom, X. R. Li, and T. Kirubarajan, *Estimation with applications to tracking and navigation: theory algorithms and software*. John Wiley & Sons, 2004.
[27] L. X. Wang, *a Course in fuzzy systems and control*, 2nd Edition Prentice-Hall press, USA, 1999.